https://dx.doi.org/10.1016/j.trd.2024.104117

Sustainable Microwave-heating Healing Asphalt Concrete Incorporating Functional Aggregates and Waste Ferrite

Dong Lu [a,b], Chaoliang Fu [c], Xi Jiang [a,*], Zhaojie Chen [a], Fulin Qu [d], Yanlin Huo [b], Zhen Leng [a,*], Jing Zhong [b,*]

[a] *Department of Civil and Environmental Engineering, The Hong Kong Polytechnic University, Hong Kong SAR*

[b] *School of Civil Engineering, Harbin Institute of Technology, Harbin, 150090, PR China*

[c] *Institute of Highway Engineering, RWTH Aachen University, Aachen, North Rhine-Westphalia 52074, Germany*

[d] *School of Civil and Environmental Engineering, University of Technology Sydney, NSW 2007, Australia*

Corresponding authors. xijiang@polyu.edu.hk (X. Jiang); zhen.leng@polyu.edu.hk (Z. Leng); zhongjing@hit.edu.cn (J. Zhong).

Abstract

Self-healing asphalt concrete can reduce maintenance costs and extend the lifespan of asphalt pavements. To advance the self-healing technique, this paper proposes a pioneering approach involving a dual microwave-heating pathway to produce a type of microwave-heating healing asphalt concrete that can offer better self-healing ability. Throughout the healing process, limestone powder filler is substituted with a waste microwave-sensitivity ferrite powder filler, primarily remedying microcracks within asphalt mastic. Additionally, the conventional aggregate is substituted with a functional aggregate to establish a three-dimensional thermally conductive framework under microwave radiation, effectively repairing microcracks at the aggregate-asphalt interface. The experimental findings reveal that the optimized formulation retains a substantial healing index of 70% after undergoing three damage-healing-damage cycles, with a reduction of 4% in crack resistance. These findings strongly endorse the practical application of functional aggregates and waste ferrite in asphalt concrete, resulting in enhanced maintenance efficiency and fostering the sustainability of the pavement system.

Keywords*:* Asphalt pavement; Microwave-heating healing; Ferrite; Solid waste recycling; Sustainable construction

1. Introduction

Porous asphalt (PA) concrete has been extensively applied in road construction because of its numerous advantages, such as mitigating issues like "drifting", "splashing", and "night glare" during rainy days (Zhu et al., 2019). These benefits improve road safety by exhibiting excellent permeability, partially absorbing traffic noise, and minimizing the "heat island effect" commonly experienced in urban areas (Ashish et al., 2023; Huang et al., 2022; Liu, D. et al., 2023; Ma et al., 2021; Zhu et al., 2019). However, the issue of water entrapment in PA concrete remains a prevalent concern due to factors such as surface tension, capillary action, and the presence of semi-connected voids (Apeagyei et al., 2014; Zhu et al., 2019). This trapped water can lead to the weakening of the bonding strength between asphalt and aggregate over time, caused by water erosion and traffic loading (Zhu, X. et al., 2020). Consequently, microcracks can form, which if left unrepaired, can expand and develop into macrocracks, significantly impacting the functionality and lifespan of the asphalt pavement (García, 2012; Jiang et al., 2021; Lu et al., 2023d). Additionally, frequent maintenance activities contribute to a substantial carbon footprint (Gong et al., 2024; Jiang, X. et al., 2022; Karimi et al., 2021; Lu et al., 2023c; Schlangen and Sangadji, 2013). As such, there is growing attention from both industry and academia towards the detection and healing of microcracks in asphalt composites, as a means to restore their properties and prolong the lifespan of pavements.

Asphalt, due to its viscoelastic nature, can autonomously heal microcracks during periods of rest (Anupam et al., 2022; García, 2012; Jahanbakhsh et al., 2018; Zhu et al., 2017). This healing process involves stress relaxation and spontaneous interfacial healing at the crack area, which reduces surface-free energy and ultimately seals the cracks (Ma et al., 2017; Zhu, H. et al., 2020; Zhu et al., 2017). However, the inherent self-healing capacity of asphalt binder is limited and may not be fully realized in pavement that is constantly subjected to traffic flow, as well as the slow migration rate of asphalt molecules (Tan et al., 2012; Xu et al., 2018). In recent years, increasing the temperature of asphalt has been widely accepted to accelerate the migration rate of asphalt molecules, thereby improving the potential for crack healing (Anupam et al., 2022; Franesqui et al., 2017).

Previous reports have indicated that the crack-healing efficiency of asphalt concrete highly depends on the heating source, i.e., external energy source (Liu et al., 2017; Wang et al., 2022; Yang et al., 2023) and concrete composition, i.e., type of aggregate, filler, and functional material (Karimi et al., 2021; Lu et al., 2024a; Wan et al., 2023). At the current stage, two common external heating sources to improve the healing process of asphalt concrete are microwave radiation heating and electromagnetic induction heating (Amani

et al., 2020; Karimi et al., 2018; Li et al., 2018b; Liu et al., 2013). Notably, microwave heating technology emerges as a superior, energy-efficient, consistent, and environmentally friendly alternative to electromagnetic induction heating for the thermal rehabilitation of asphalt pavements (Liu, Jianan et al., 2022; Phan et al., 2018). Given these inherent advantages, microwave heating is a more feasible option for increasing the asphalt concrete's crack-healing efficiency.

In addition to the heating method, the composition of asphalt concrete plays a crucial role in enhancing its crack-healing efficiency, consequently, three widely employed strategies are implemented to optimize the asphalt concrete composition (Liu, Jianan et al., 2022; Wan et al., 2023; Wang et al., 2022; Zhu et al., 2019): 1) the direct combination of functional additives with asphalt, followed by their integration with aggregate (filler) to create functional asphalt-based concrete; 2) the substitution of limestone powder (LP) filler with microwave-sensitive filler, resulting in functional filler-based asphalt concrete; and 3) the utilization of steel slag (SS) aggregate as a replacement for natural aggregate, ultimately forming functional aggregate-based asphalt concrete. Notably, the first two strategies primarily heal cohesion failure within the asphalt mastic, as the added functional additives generate heat and soften the asphalt when exposed to microwave radiation. However, it should be considered that asphalt or filler only makes up approximately 5% of the total volume of asphalt concrete, resulting in limited improvement in heating-healing efficiency (Zhu et al., 2019). Additionally, the random distribution of SS aggregate in asphalt concrete can soften the surrounding asphalt mastic under microwave radiation, addressing primarily the bonding failure between the aggregate and asphalt (Liu, Jinzhou et al., 2022; Xu and Wang, 2016). However, implementing SS aggregate often involves partial substitution for natural aggregate with specific particle sizes, which would result in localized overheating, as well as the need for intricate grading and aging procedures further complicating the practical applications (Liu, Jianan et al., 2022). Currently, there is a significant lack of research dedicated to achieving high-efficiency and uniform heat generation/transfer pathways within asphalt composite. This deficiency hinders the efficient simultaneous healing of both cohesion failure and bonding failure in asphalt concrete.

To tackle the previously mentioned issue, we have successfully developed a novel functional aggregate with remarkable microwave heating potential (Lu et al., 2023a; Lu et al., 2023b). The creation of this functional aggregate involves the application of a nanocoating comprised of carbon nanotube polymer (CNTP) nanocomposite onto the surface of the aggregate. This nano-coating enables efficient and precise repair of microcracks specifically at the interface between the aggregate and the asphalt. Importantly, the functionalization process we have developed allows for nano-coating to be applied to aggregates of any

size, enhancing its versatility and applicability. To further enhance the healing effect of asphalt composite, ferrite powder (FP) is utilized in this study. FP is chosen for its rich composition of microwave-sensitive metal oxides, such as Fe_2O_3 and ZnO, which effectively convert electromagnetic waves into heat. Notably, FP shares a similar particle size and softness with limestone powder (LP) filler, rendering it a potential substitute for LP filler in asphalt concrete (Nabiun and Khabiri, 2016). Therefore, FP filler proves to be an ideal candidate for replacing LP filler and integrating it with other components to facilitate the repairing of microcracks inside the asphalt mastic. In addition to its advantageous properties, FP is a significant component of the solid waste generated from iron production (Leclerc et al., 2003). By recycling FP in asphalt pavements, several benefits can be achieved. It helps to reduce the amount of waste generated from iron production, thereby minimizing the environmental impact associated with its disposal. This aligns with the principles of sustainability and waste reduction. Furthermore, the inclusion of FP filler in asphalt pavements improves their mechanical and durability properties (Nabiun and Khabiri, 2016), resulting in decreased maintenance requirements and an extended lifespan for the infrastructure. However, it is worth noting that there is a research gap exploring the combined use of functional aggregate and microwave-sensitive FP filler to achieve efficient simultaneous healing of cohesion failure and bonding failure in asphalt concrete, as well as mitigating carbon footprint.

To fill this research gap, this paper proposes a pioneering approach involving a dual microwave-heating pathway to produce a novel type of microwave-heating healing asphalt concrete that can offer higher repair efficiency. The incorporation of functional aggregate can construct a three-dimensional thermally conductive framework inside the asphalt concrete when exposed to microwave radiation, targeted and effectively heals microcracks at the aggregate-asphalt interface. In addition, the microcracks in asphalt mastic can be repaired with the help of microwave-sensitive FP filler. The surface properties, composition and morphology, and the microwave-heating behavior of the functional additives are studied to uncover their potential for microwave-heating healing applications in asphalt pavements. Additionally, the cracking resistance, microwave heating behavior, and microwave heating-healing ability of microwave-heating healing asphalt concrete are evaluated to explore its practical application prospects.

2. Experimental details

2.1. Materials

PA concrete is widely recognized for its eco-friendliness and versatility, making it a popular choice for surfacing pavements, particularly in densely populated urban areas like Hong Kong (Jiang, J. et al., 2022;

Lu et al., 2023b). Therefore, in this study, PA-13 was selected as the base concrete and empowered with microwave-heating healing capability to effectively address asphalt pavement raveling. Coarse and fine aggregates were obtained from crushed granite, and their aggregate gradation can be found in **Fig. 1**. To enhance the functionality of the aggregates, a nanocomposite of carbon nanotube polymer (CNTP) was synthesized through meticulous mechanical mixing of a CNT solution and liquid polyacrylic acid, which was then applied as a coating on the aggregate surface. **Table 1** summarizes the main characteristics of the PG 76/22 asphalt. Additionally, asphalt concrete was fabricated using limestone powder (LP) filler and ferrite powder (FP) filler. **Table 2** shows that the FP filler has a density and specific gravity almost twice that of the LP filler, mainly due to its higher Fe_2O_3 content (over 45%).

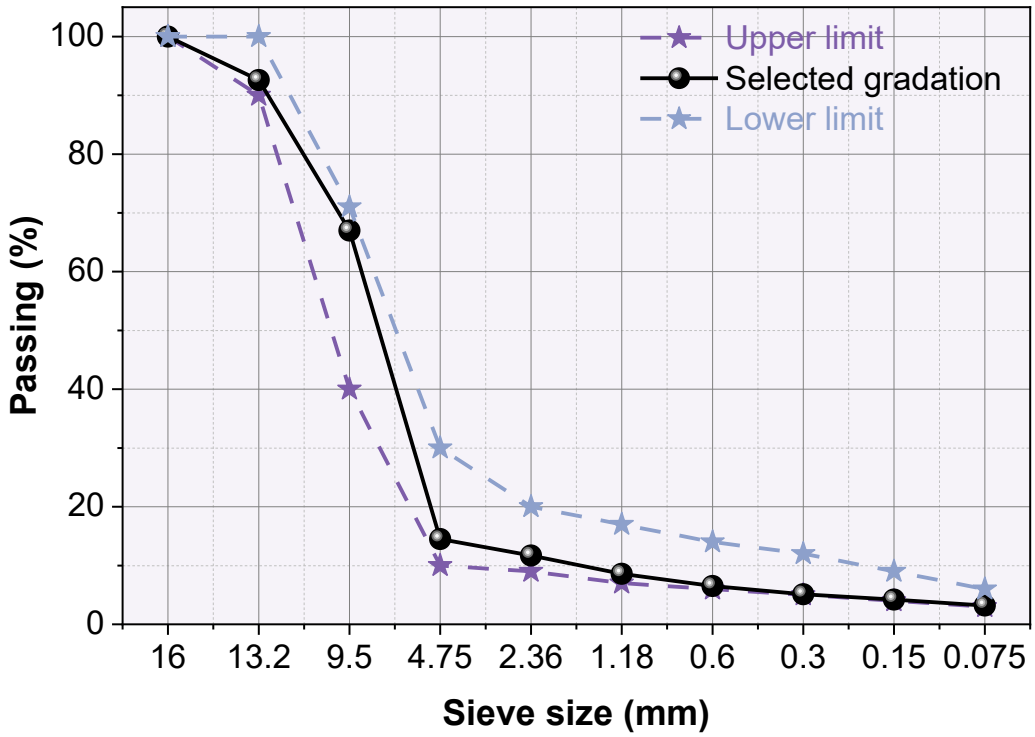

Fig. 1. Gradation of aggregate used for preparing porous asphalt (PA-13) concrete.

Table 1 Main properties of PG 76/22 asphalt.

Technical properties	Value	Test methods
Penetration at 25 °C (0.1 mm)	46	T 0604
Softening point (°C)	93	T 0606
Viscosity at 135 °C (mPa·s)	2450	T 0625

131 **Table 2** Properties of fillers.

Filler type	Density (g/cm^3)	Specific surface area (m^2/g)	Fineness modulus	Specific gravity
LP	2.716	0.913	5.12	2.25
FP	5.346	2.110	2.85	5.36

132 ***2.2. Development of functional aggregate and asphalt concrete***

133 To manufacture the functional aggregate, a CNTP functional film with high microwave sensitivity was
134 applied to the surface of the aggregate using a coating process. The coated aggregate, along with heated
135 asphalt and filler, was then mixed together to create asphalt concrete samples. As depicted in **Fig. 2**, the
136 synthesis of a well-dispersed CNTP mixture involved a comprehensive shear mixing process, combining a
137 5% solid content CNT dispersion with a 48% solid content polyacrylic acid solution. The raw aggregates
138 were then immersed in the well-dispersed CNTP mixture, and subsequently manually stirred at 30-50 r/min
139 for 10 minutes to achieve a uniform coating of CNTP on the aggregate surface. For a more detailed
140 explanation of this process, please refer to our earlier publication (Lu et al., 2023b). The CNTP film used
141 for coating the aggregate surface contains approximately 20 wt% CNT, which helps reduce CNT
142 agglomerations commonly observed in conventional processes and maintains good thermal conductivity
143 when exposed to microwave radiation. This is critical because if CNTs are mixed directly with asphalt, the
144 CNTs will inevitably agglomerate (Eisa et al., 2022), which may lead to localized overheating of the asphalt
145 concrete, thus affecting its thermal conductivity. In this study, the mixture design of PA-13, as depicted in
146 **Table 3**, was used for the asphalt concrete. The asphalt-aggregate ratio and the target air void specifications
147 for the PA-13 concrete were determined as 3.9 and 23±0.5 %, respectively, according to our previous
148 research (Jiang, J. et al., 2022; Lu et al., 2023b).

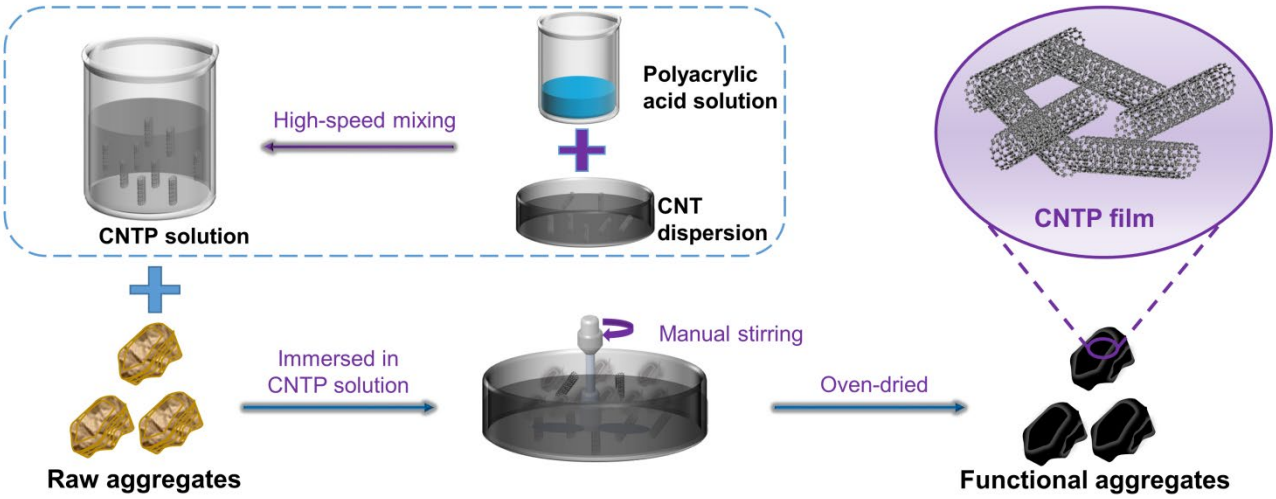

Fig. 2. Illustration of coating CNTF film on the surface of aggregates.

149

150 **Table 3** Mixture design of PA-13 (%).

Mixture ID	Aggregate		Filler	
	Raw	Functional	LP	FP
PA-0FP	100	0	100	0
PA-50FP	100	0	50	50
PA-100FP	100	0	0	100
PA-FAg-0FP	0	100	100	0
PA-FAg-50FP	0	100	50	50
PA-FAg-100FP	0	100	0	100

151 Note: The LP filler has been replaced with the FP filler using an equivalent volume approach. FAg represents the functional
152 aggregate.

153

2.3. Laboratory testing

2.3.1. Characterization of aggregate and filler

The SEM observations were carried out after the samples were prepared by oven-drying at 60℃ for 2 days. This drying process helps remove any moisture from the samples and ensures accurate observations of their morphology. In order to improve the electrical conductivity of the samples and mitigate charging effects during SEM analysis, a thin layer of gold (Au) was sputtered onto the sample surfaces, as recommended by our previous work (Lu et al., 2024b). This gold coating helps improve the image resolution and provides a conductive surface for electron imaging. Raman spectra were obtained using a confocal Raman spectrometer with a 532 nm laser excitation source. The water absorption of aggregates was tested according to the *Chinese National Standard JTG E42-2005.* The thermal characteristics of the filler and aggregate were examined using microwave heating. The samples were heated in an 800 W microwave device for different durations to assess their response to heat. The surface temperatures of the samples were collected using an infrared thermal imager, allowing for the evaluation of their thermal behavior. To determine the electromagnetic parameters of the fillers, a microwave vector network analyzer system was used. As recommended by Liu et al. (Liu, J. et al., 2023), the electromagnetic parameters of the fillers were tested using a microwave vector network analyzer system with a frequency of 1-18 GHz.

2.3.2. Cracking resistance

The cracking resistance of asphalt concrete was assessed using a semi-circular bending (SCB) test, as shown in **Fig. 3**. To carry out the test, six semi-circular samples were prepared for each group, with dimensions of 150 mm in diameter, 50 mm in thickness, and 75 mm in height. To minimize potential errors, the average value of the testing results was recorded. A notch, measuring 1.5 mm in width and 15 mm in height, was created in the center of each semi-circular specimen (AASHTO Designation: TP 124-161). All experiments were conducted at a temperature of 25℃ and a loading rate of 0.5 mm/min, as recommended by previous studies (Amani et al., 2023; Mojabi et al., 2020).

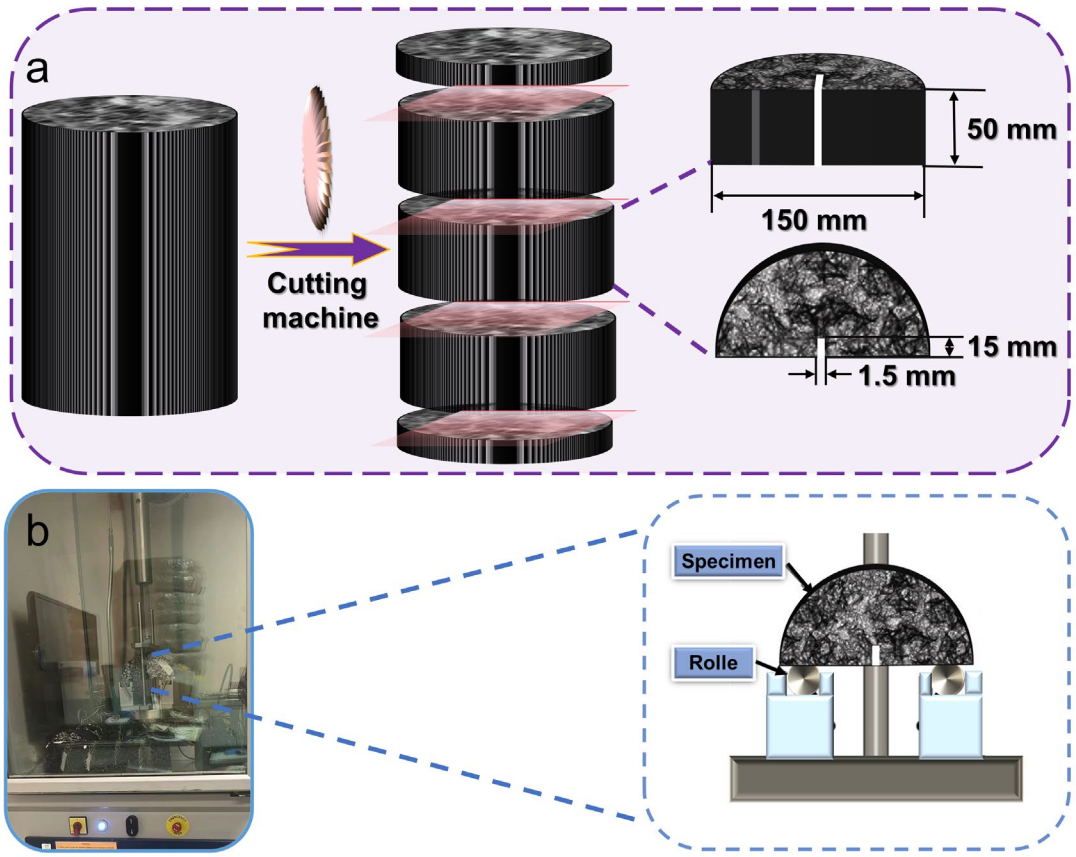

Fig. 3. Illustration of SCB test: (a) preparation procedure of specimens and (b) testing set-up.

179 *2.3.3. Microwave heating behavior*

180 According to our previous study (Lu et al., 2023b), the asphalt concrete samples were subjected to
181 microwave heating in an oven to investigate their microwave heating behavior. The surface temperatures
182 of the samples were recorded using an infrared thermal imager. The specimens were treated at different
183 times at a power of 800 W. This methodology aimed to identify the most optimal heating parameters for
184 the subsequent healing procedure. The heating rate (V_H, ℃/s) of the specimens was obtained using
185 **Equation (1)**.

186 $$V_H = \frac{T - T_0}{t} \quad (1)$$

187 where T_0 stands for the initial temperature of the samples (℃), T represents the temperature of the
188 samples after microwave radiation (℃), and t stands for the microwave radiation duration (s).

189 *2.3.4. Damage-healing-damage (D-H-D) procedure*

190 According to our previous experience (Lu et al., 2023b), a typical damage-healing-damage (D-H-D)
191 cycle test was adopted to evaluate the healing efficiency of the asphalt composite, as illustrated in **Fig. 4.**

The asphalt concrete sample with pre-cut crack was then subjected to an SCB test. Following the test, the two sections of the specimen were carefully reassembled and microwave-heated at a power of 800 W. After heating, the concrete samples were left at room temperature for a 6-hour resting period. Finally, the specimens were subjected to another SCB test, thereby finishing a full process. The healing index (*HI*, %) of the samples was calculated through **Equation (2)**.

$$HI = \frac{F_1}{F_0} \times 100\% \quad (2)$$

where F_0 and F_1 are the peak force of asphalt concrete before and after healing (N), respectively.

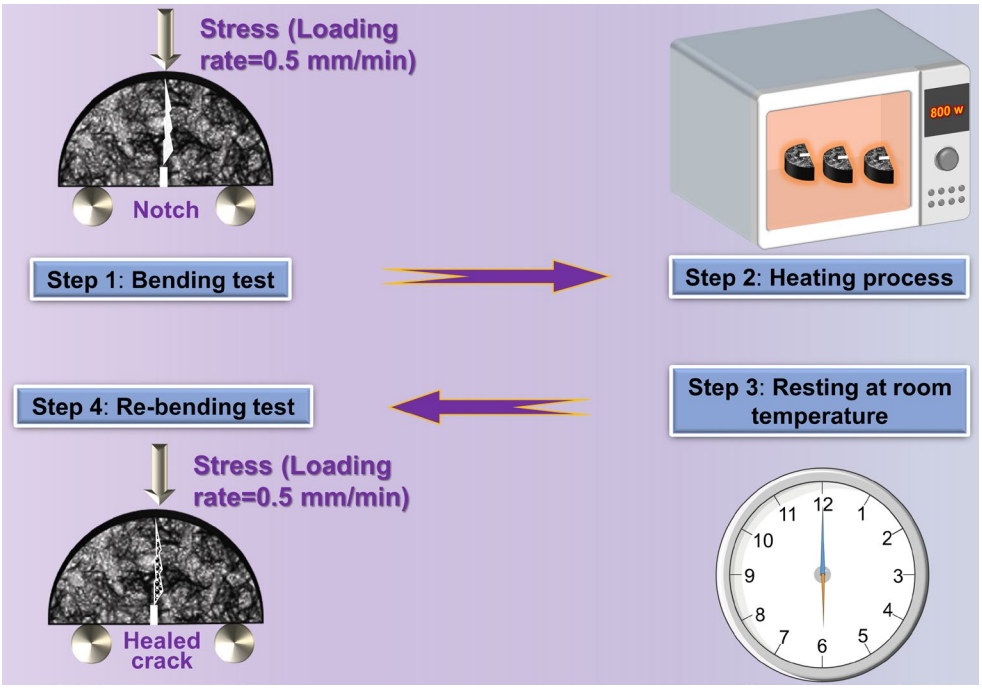

Fig. 4. Illustration of concrete undergoing one D-H-D cycle.

2.3.5. Microcrack observation

The use of X-ray computed tomography (X-CT) in analyzing the microcrack evolution of asphalt concrete during the D-H-D cycle is a non-destructive and advanced approach. In this study, a multiscale-Voxel series XT H225 ST industrial X-CT machine was employed for scanning purposes. After scanning, a total of 520 images were collected and then reconstructed. The reconstructed images were then analyzed using VGSTUDIO MAX software to study the microcrack evolution. This software provides the necessary tools and functionalities to examine and understand the changes in the microcracks over time. By utilizing X-CT and advanced software analysis, researchers can gain valuable insights into the behavior of asphalt concrete under different loading conditions and the effectiveness of healing processes.

3. Results and discussion

3.1. Characteristics of aggregate and filler

In this section, the focus is on studying the characteristics of functional additives with regard to their potential for microwave-heating healing applications. Several aspects are investigated, including surface properties, composition and morphology, and microwave-heating behavior.

3.1.1. Morphology and chemical compositions of functional additives

The raw aggregate, as shown in **Fig. 5a**, appears grey in color. However, after being dip-coated with the CNTP functional film, the functional aggregate exhibits uniform darkness. In addition, SEM images reveal a transformation in the morphology of the aggregate, where the neat surface is replaced by a textured CNTP layer. Particularly noticeable are the well-connected bundles of CNT, as depicted in **Fig. 5b**. The successful dip-coating of the CNTP functional layer onto the aggregate surface is further supported by the presence of a G/D peak (band) and a minor 2D peak (band) in the Raman spectrum, as depicted in **Fig. 5c**. In **Fig. 5d**, a slight decrease of 7.4% in the 24-hour water absorption of the functional aggregate is illustrated compared to the raw aggregate. This decrease can be attributed mainly to the hydrophobic characteristic of the CNTs (Lu et al., 2022). To prepare the functional CNTP film with excellent microwave absorption ability and strong adherence to the aggregate surface, a polymer binder consisting of the polyacrylic acid solution was employed in combination with CNT in this design. According to our experience (Lu et al., 2023a), a 20 wt% CNT content was used in the CNTP composite, wherein the dominant CNT in the coating film improves the interlocking between asphalt and aggregate and fosters direct contact between functional aggregates. As a result, well-connected three-dimensional (3D) functional skeletons are formed in the asphalt concrete.

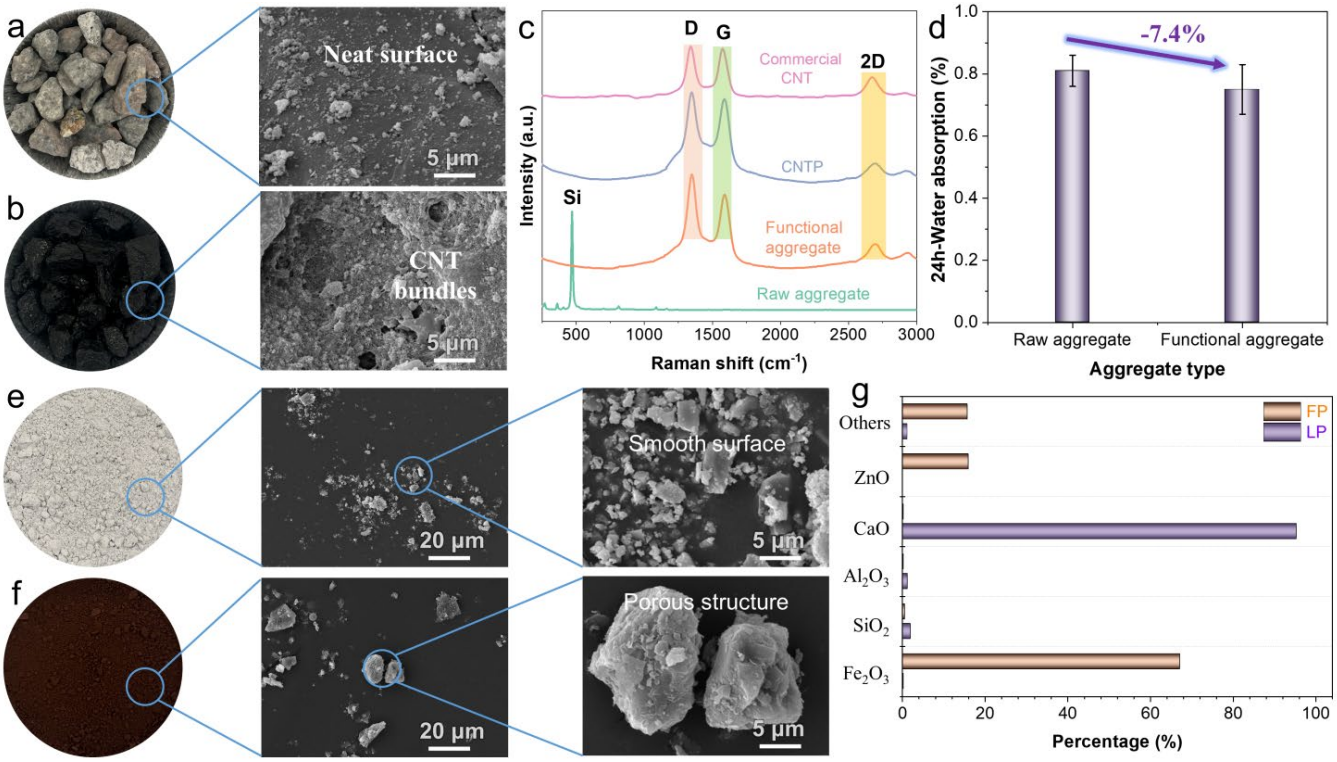

Fig. 5. Characteristics of aggregate and filler: appearance and SEM images of (a) raw aggregate and (b) functional aggregate; (c) Raman spectrum and (d) water absorption of aggregate; appearance and SEM images of (e) LP and (f) FP filler; and (g) chemical compositions of fillers.

In **Fig. 5e**, the LP filler is characterized by a grey-white color, and SEM images reveal that it exhibits an irregular polyhedral shape with prominent bumpy structures. Conversely, the FP particles display a dark brown hue, and their SEM images demonstrate a porous structure, as depicted in **Fig. 5f**. XRF analysis results indicate an impressive CaO content of 95.4% in the LP filler, as shown in **Fig. 5g**. On the contrary, the FP filler contains a higher content of metal oxides such as Fe_2O_3 and ZnO compared to the LP filler. This compositional difference allows the FP filler to efficiently convert electromagnetic waves into heat upon exposure to microwave radiation (Lu et al., 2024a). Consequently, the FP filler exhibits exceptional microwave heating ability, ensuring rapid microwave heating in asphalt composites.

3.1.2. Microwave heating ability of functional additives

Fig. 6a illustrates that both fillers and aggregates were subjected to microwave radiation, and their surface temperatures were subsequently measured using an infrared camera. In **Fig. 6b**, it can be observed that the surface temperature of the raw aggregate fluctuates slightly at different durations of microwave radiation. For instance, when exposed to 180 seconds of radiation, the surface temperature of the raw

aggregate only increases by approximately 25°C. This modest temperature rise is because the raw mineral aggregate is not sensitive to electromagnetic microwaves, resulting in limited microwave heating capability. In contrast, the surface temperature of the functional aggregate undergoes a more substantial increase. It reaches approximately 90°C after only 30 seconds of radiation and further climbs to around 110°C as the radiation duration is increased to 60 seconds. These findings indicate that the addition of functional aggregate can effectively soften the coated asphalt with the assistance of microwave radiation. Furthermore, the temperature of the LP filler reaches approximately 35°C and 65°C after 60 seconds and 180 seconds of heating, respectively. On the contrary, the FP filler experiences a rapid increase in surface temperature to about 105°C after 60 seconds of radiation. As mentioned in section 2.1, the softening point of the asphalt is approximately 93°C. Therefore, the temperature attained by the FP filler, which is higher than the softening point, is sufficient to effectively soften the surrounding asphalt.

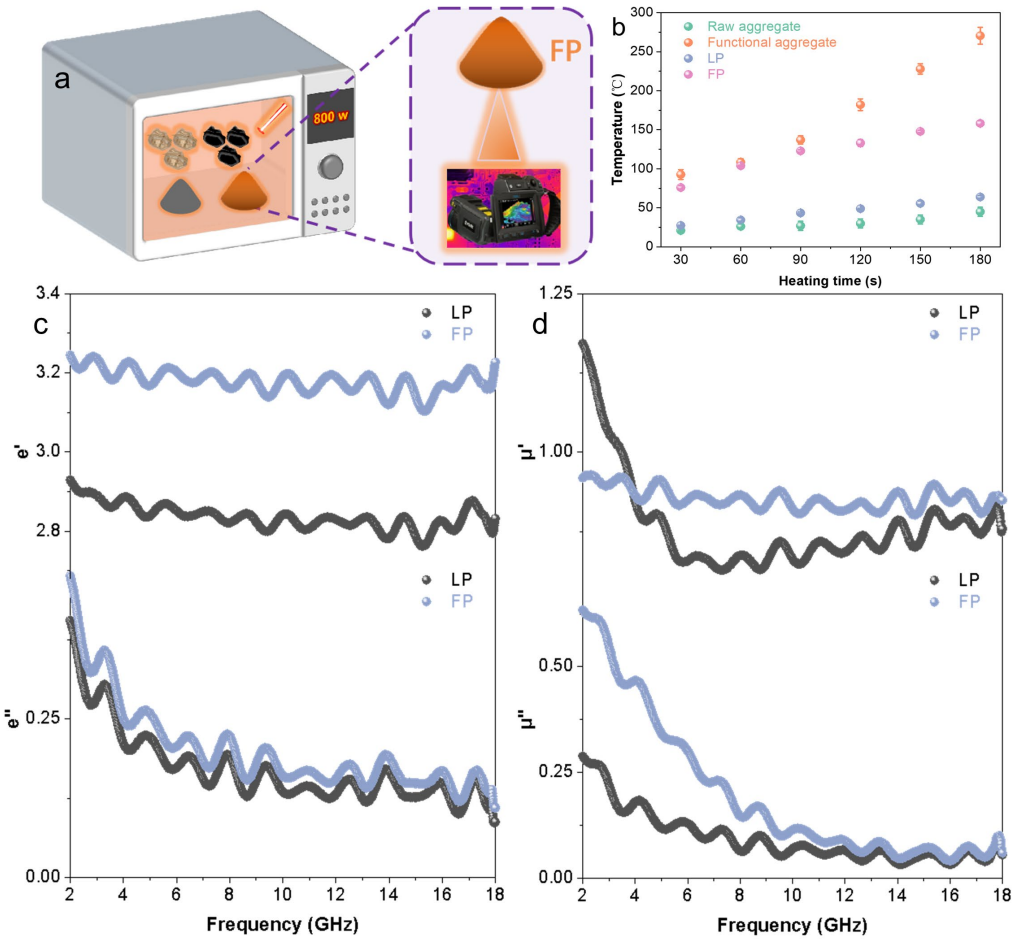

Fig. 6. (a) Illustration of surface temperature collection of raw materials under radiation; (b) the temperature of raw materials; the electromagnetic parameters of the filler: (c) real parts (**e'**) and imaginary parts (**e''**) of the complex permittivity; and (d) real parts (**μ'**) and imaginary parts (**μ''**) of the relative complex permeability.

The previous studies highlighted that the ability of an electromagnetic wave to be converted into heat is directly related to the values of the electromagnetic parameters (Liu, J. et al., 2023; Lou et al., 2021). Specifically, the real and imaginary parts of the complex permittivity and their relative complex permeability play a crucial role in this conversion process (Liu, J. et al., 2023; Lou et al., 2021). As shown in **Fig. 6c** and **Fig. 6d**, the real and imaginary parts of the complex permittivity of the LP filler fall within the range of 2.8-3.0 and 0.1-0.4, respectively. These values reflect the insensitivity of LP to microwave radiation. In contrast, the real and imaginary parts of FP filler's complex permittivity and relative complex permeability are all significantly higher than those of LP, suggesting that FP has considerable potential as a magnetic loss microwave absorber. The presence of magnetic components, such as Fe_2O_3 and ZnO, contributes to this potential. These components can effectively absorb microwave radiation through phenomena like domain wall resonance, natural resonance loss, and other magnetic polarization functions. The outstanding dielectric parameters of FP contribute to its remarkable heating-healing properties. Based on the obtained results, it can be concluded that both functional aggregate and FP filler show promising abilities to enhance efficient thermal formation and uniform thermal transfer in asphalt composites. Consequently, the combination of functional aggregate and FP filler in asphalt concrete holds significant potential to improve its microwave-heating healing efficiency, while also offering environmental and economic advantages.

3.2. Cracking resistance

In **Fig. 7a**, it can be observed that the asphalt concrete modified with 50% FP exhibits the highest peak force among all the samples. This indicates that adding 50% FP filler to asphalt concrete results in optimal resistance against cracking. The enhanced ability to resist cracking can be mainly attributed to the synergistic effects of using 50% FP and 50% LP filler, which can refine the microstructure of the asphalt composite. Additionally, the porous structure of FP filler allows for greater absorption of the asphalt on its surface, thereby enhancing the bonding strength with the aggregate. It is worth noting that the peak force of the PA-100FP specimens is slightly smaller compared to the PA-50FP specimens but still higher than that of the plain PA-0FP specimens (**Fig. 7b**). Therefore, it can be concluded that the optimum replacement ratio of FP in asphalt composite is 50% to achieve the optimal cracking resistance. Additionally, the peak force of asphalt concrete with functional aggregate decreases by 10.3% compared to plain asphalt concrete specimens. Nevertheless, the simultaneous utilization of FP and functional aggregate in asphalt concrete can offset this decrease in peak force, as demonstrated by the PA-FAg-50FP (1506 N) and PA-FAg-100FP (1370 N) specimens. The above findings suggest that the combined application of FP and functional

aggregate in asphalt concrete yields satisfactory cracking resistance, enabling it to be acceptable for practical applications.

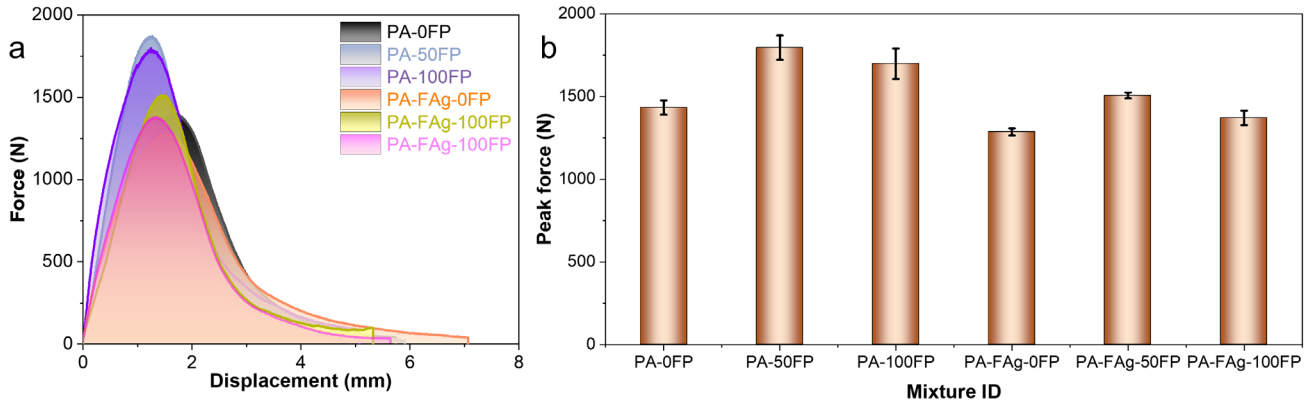

Fig. 7. (a) Load-displacement curves and (b) the peak force of asphalt concrete.

3.3. Microwave heating behavior

In this study, the asphalt composite's average surface temperature was collected to assess its heating ability. According to the results presented in **Fig. 8a**, the surface temperature of PA-50FP specimens increases by 30-60℃ compared to that of the PA-0FP specimens. This temperature increase is primarily because of the presence of metal oxide components in the FP filler, indicating that the addition of FP filler enhances the microwave heating ability of the concrete. Notably, the temperature obtained during microwave radiation does not reach the necessary level to fully soften the surrounding asphalt. It is remarkable that the PA-FAg-100FP specimen reaches about 95℃ after just 30 seconds of heating, which corresponds to the softening point of the asphalt used in this study. Due to this significant finding, a microwave time of 30 seconds was selected to evaluate the microwave heating capability of the various groups of asphalt concrete. Notably, the surface temperature of the asphalt concrete containing 100% steel slag only reached 20℃ after 30 seconds of microwave irradiation (Liu, Jianan et al., 2022), highlighting the superior microwave-heating efficiency of our formulation. Note that some samples in PA-FAg-50FP and PA-FAg-100FP groups appear to collapse after 90 seconds of microwave heating, so temperature data for these specimens are not collected. This emphasizes the importance of appropriately controlling the microwave heating time.

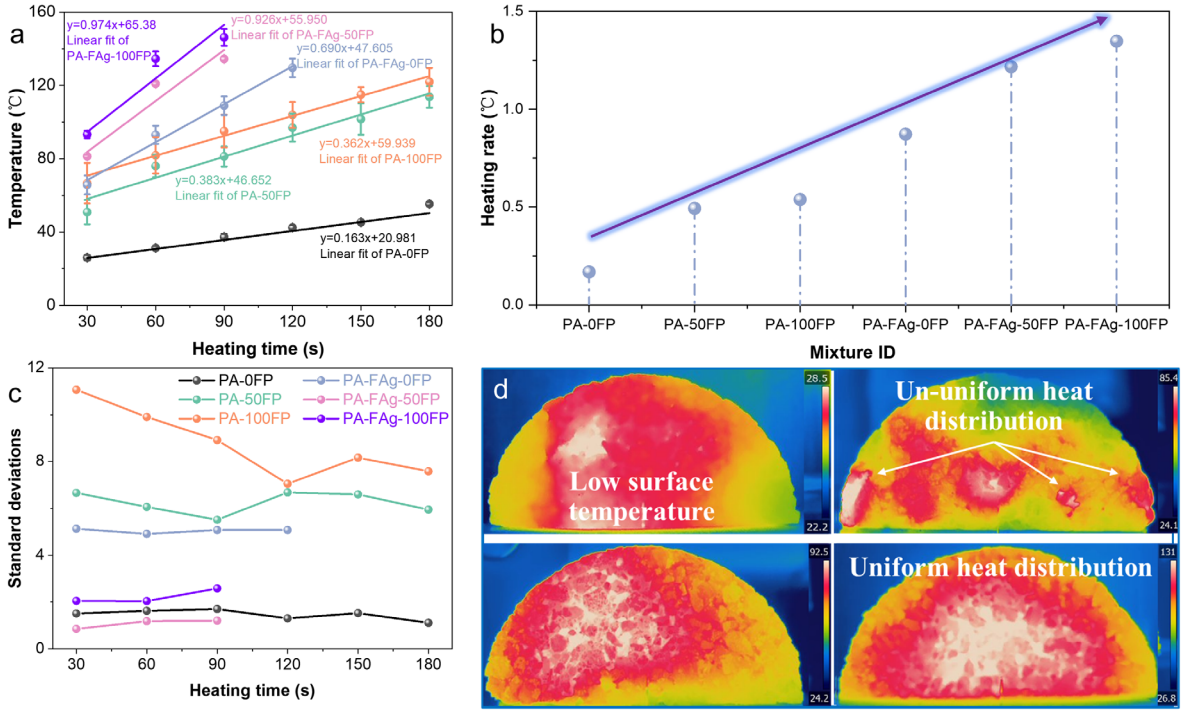

Fig. 8. Temperature of samples: (a) the relationship between temperature and time; (b) heating rate; (c) standard deviation of temperature data; and (d) infrared thermal images of PA-0FP (upper left), PA-100FP (upper right), PA-FAg-0FP (bottom left), and PA-FAg-100FP (bottom right) samples after 60 seconds of microwave radiation.

According to the findings depicted in **Fig. 8b**, the microwave heating rates of the PA-FAg-50FP and PA-FAg-100FP specimens are 1.217 ℃/s and 1.347 ℃/s, respectively. These values are notably higher than the heating rates reported in previous studies (Li et al., 2018a; Lou et al., 2020). This indicates that the microwave heating method employed in this study achieves significantly higher heating efficiency. Furthermore, the standard deviation (SD) data of the sample's surface temperature can be used to evaluate heating uniformity. Specifically, the SD values of the surface temperature for the PA-0FP samples fall within the range of 1.1-1.7℃ (**Fig. 8c**). In contrast, the PA-50FP and PA-100FP specimens exhibit higher SD values relative to the PA-0FP specimens, indicating that replacing LP with FP filler can result in a non-uniform distribution of microwave heating, primarily due to the agglomeration of the admixed FP filler in asphalt concrete. This agglomeration leads to localized overheating in certain regions of the asphalt concrete, especially in higher concentrations of FP-modified asphalt concrete, while other regions with lower concentrations of FP filler experience slower microwave heating. This finding can be further supported by the infrared thermal images provided in **Fig. 8d**. Additionally, the PA-FAg-0FP specimens present SD values of around 5.0℃, whereas the SD values of the PA-FAg-50FP and PA-FAg-100FP decrease to 1.0-2.0℃. This indicates that the functional aggregate, when combined with microwave-sensitive FP filler, not

only enhances heat generation but also facilitates heat transfer to the surrounding components.

3.4. Microwave-heating healing ability

As shown in **Fig. 9a**, it is evident that the peak force of all the concrete groups decreases as the number of D-H-D cycles increases. Furthermore, the calculated HI values for each group of samples are presented in **Fig. 9b**. The PA-0FP specimens experience a significant decrease in HI values to 15.1% after three D-H-D cycles, indicating that these specimens have poor heating-healing abilities under microwave radiation. On the other hand, all FP-modified composites exhibit higher HI, suggesting an improved microwave heating-healing efficiency relative to the PA-0FP specimens, mainly attributed to the better microwave absorption capacity of FP in comparison to LP. As reported in section 3.1.2, FP indeed possesses higher electromagnetic parameters than that of the LP filler, suggesting its superior capability to absorb electromagnetic waves under radiation. The efficient conversion of electromagnetic losses to heat in the FP-modified mixture provides it with a beneficial healing ability. For instance, the PA-50FP and PA-100FP specimens exhibit HI of approximately 40% and 45%, respectively, after undergoing three D-H-D cycles. However, it is important to note that solely introducing FP filler is not the most effective approach for enhancing the healing capability of the asphalt composites, due to the limited proportion (~5%) of filler present in the asphalt composite.

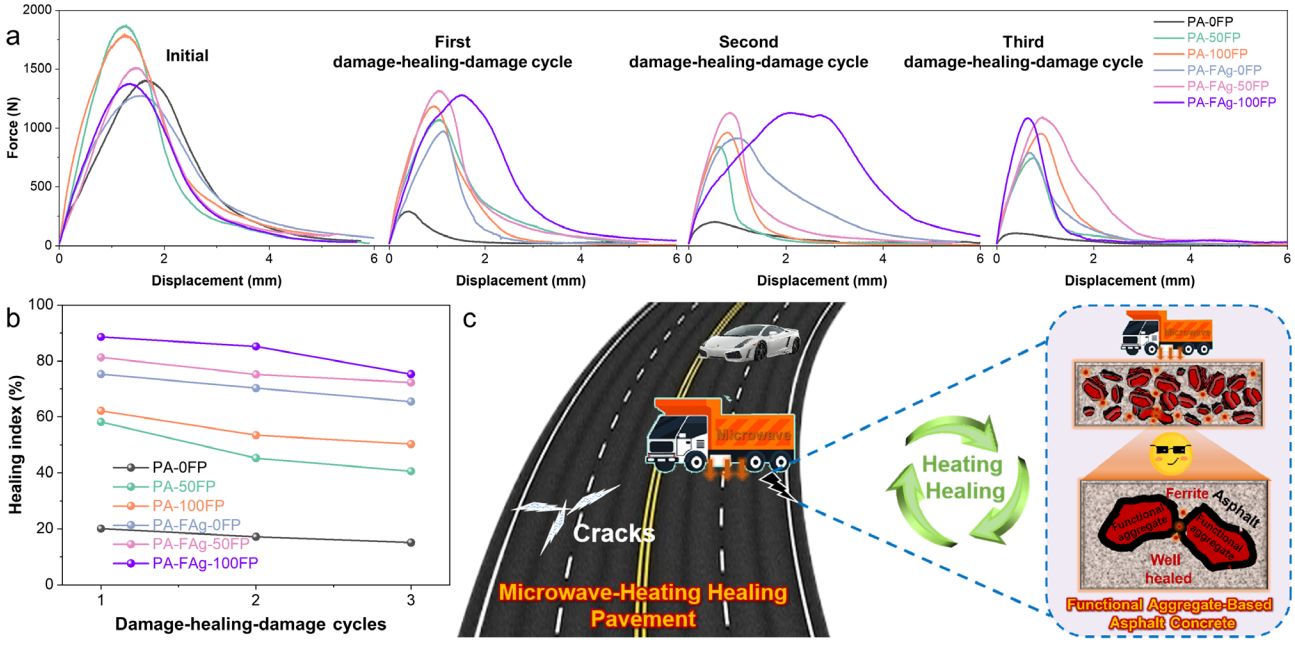

Fig. 9. The microwave-heating healing behavior of asphalt composite: (a) loading force; (b) HI; and microwave heating-healing pavement with the presence of functional aggregate and ferrite.

In **Fig. 9b**, it can be observed that the HI index of the functional aggregate-modified concrete reaches 75.3% after one D-H-D cycle, which decreases slightly to 65.5% after three cycles. However, it is important to note that the PA-FAg-50FP and PA-FAg-100FP concretes exhibit higher HI values of 81.3% and 88.6%, respectively, after one D-H-D cycle, far higher than that of healing level (i.e., 5-43%) of the carbon materials (e.g., carbon fiber, carbon nanotube, and carbon nanofiber) modified-asphalt concrete (Yoo et al., 2019) or strength healing ratio (i.e., 20-60%) of asphalt concrete with steel slag (Yang et al., 2022), indicating that the combination of functional aggregate with FP in asphalt concrete achieves exceptional heating-healing ability. During the healing process, the functional aggregate plays a crucial role in building a functional heating skeleton structure inside the asphalt composite. This aids in repairing the microcracks occurring at the asphalt-aggregate interface. Simultaneously, the combination of FP filler with binder helps to repair microcracks within the asphalt mastic, as depicted in **Fig. 9c**. Although there is only a slight improvement in the healing efficiency of the 100% FP-modified sample compared to the 50% FP-modified sample, it is still recommended to apply 100% FP to replace LP filler, because of the effective recycle of waste FP and the environmental and economic benefits obtained through the substitution of LP resources.

3.5. Crack evolution in asphalt concrete

The evolution of microcracks in concrete during the damage-healing process is recorded and observed using X-CT. The crack size in the PA-0FP, PA-100FP, PA-FAg-0FP, and PA-FAg-100FP specimens is compared before and after the microwave-heating healing process using X-CT, as shown in **Fig. 10a**. X-CT images clearly show the presence of cracks in the specimens before healing. To quantify the change in crack size between these specimens before and after heating, X-CT image analysis is conducted, and the crack size is measured using Nano Measurer 2.0 software. In this study, ten X-CT images are randomly chosen for each group of specimens. In each image, two regions are measured, resulting in a total of 20 data points for crack size analysis. As shown in **Fig. 10b**, the crack sizes range from 700-1100 μm for PA-0FP specimens, 500-900 μm for PA-100FP specimens, 1500-2000 μm for PA-FAg-0FP specimens, and 1000-1500 μm for PA-FAg-100FP specimens. Subsequently, the damaged specimens were exposed to microwave radiation and underwent X-CT scanning using the same parameters. The X-CT images reveal that the microcracks tend to close after microwave radiation, particularly in the case of PA-FAg-100FP specimens. Their crack size is reduced to below 100 μm, with an average crack size that is 94% lower than the initial value before healing (**Fig. 10c and Fig. 10d**). These findings suggest that the optimized design of a dual responsive heating-healing system, comprising functional aggregate and FP, has a positive effect on crack closure in asphalt concrete.

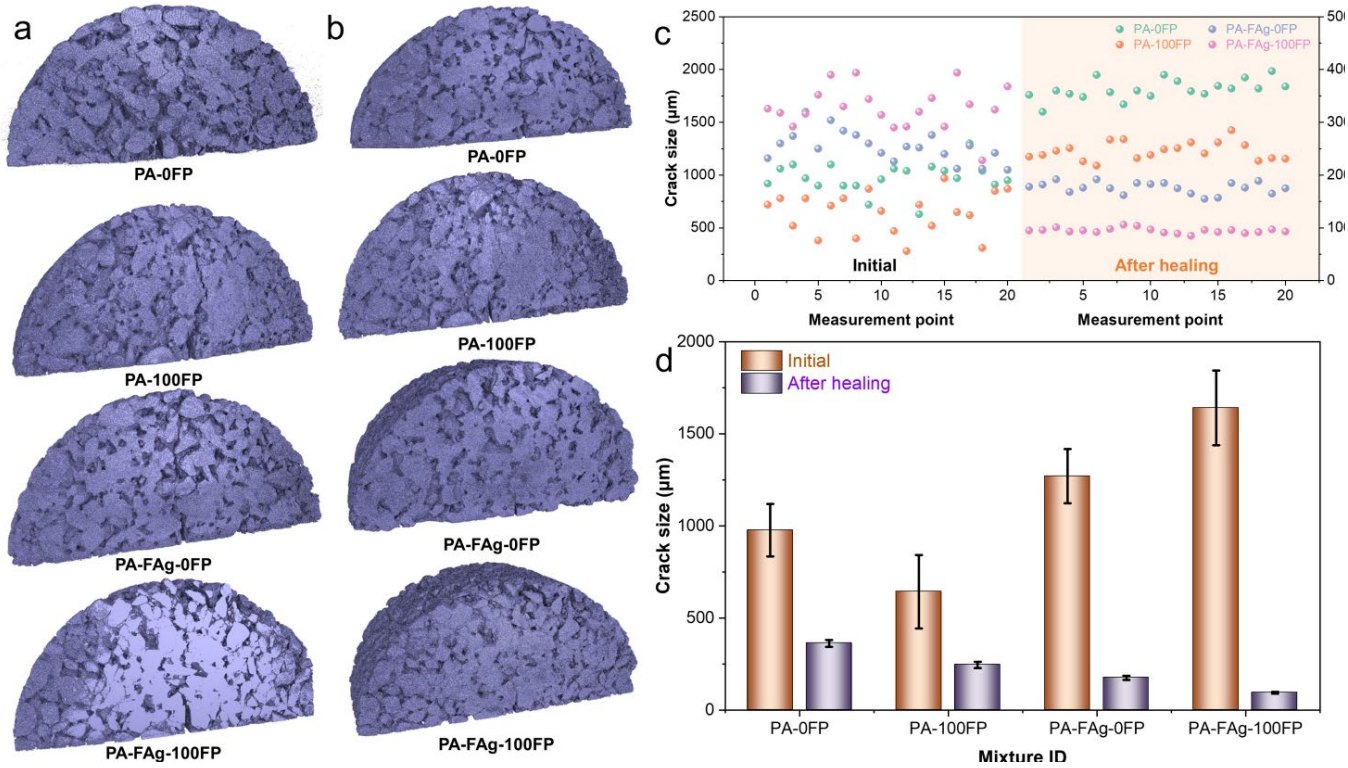

Fig. 10. Microcrack evolution of asphalt concrete during the D-H-D process: X-CT images of asphalt concrete (a) before healing and (b) after healing; (c) crack size distribution; and (d) the calculated average crack size.

4. Summaries and perspectives

In this study, a microwave-heating healing asphalt concrete with a dual microwave-heating pathway was developed. By incorporating a combination of functional aggregate and ferrite powder (FP) filler in optimized ratios, the heating-healing efficiency of the asphalt concrete is significantly improved. This optimization enhanced the overall heating process, resulting in more efficient heating and improved transfer of heat energy within the microwave-heating healing asphalt composite. Accordingly, this pioneering approach can significantly enhance the healing performance of asphalt composite. Based on the findings presented in this study, the following key conclusions can be made.

(1) The development of a dual microwave-heating pathway within the asphalt concrete effectively addresses issues related to non-uniform heat distribution under microwave radiation. Moreover, it enhances heat generation efficiency and facilitates efficient heat transfer to the surrounding areas within the asphalt concrete. In the dual microwave-heating system, a unique approach is adopted by incorporating a functional film-coated aggregate instead of the conventional aggregate. This modification creates a three-dimensional

thermally conductive framework within the asphalt concrete when exposed to microwave radiation. Furthermore, a microwave-sensitive FP filler is utilized as a replacement for the traditional limestone powder filler. The addition of the FP filler enables the generation of heat within the asphalt mastic when microwave radiation is applied. This thermal generation process enhances the healing capability of the asphalt concrete.

(2) The inclusion of functional aggregate alone in asphalt concrete results in a reduction of about 10% in peak force relative to plain asphalt concrete. However, when FP filler is combined with functional aggregate, this reduction in peak force can be compensated. In particular, the PA-FAg-50FP composite exhibits almost the same peak force as plain asphalt concrete, suggesting that the combination of FP filler and functional aggregate provides satisfactory cracking resistance for practical applications.

(3) The optimized formulation, PA-FAg-100FP, maintains its exceptional heating-healing efficiency of around 70% even after undergoing three cycles of damage-healing-damage. Additionally, there is only a minor 4% reduction in cracking resistance. This highlights the enormous potential of optimized formulation in practical scenarios, as it retains its efficient healing capabilities while maintaining good cracking resistance.

Future studies in the field of microwave-heating healing asphalt concrete can benefit from focusing on simulating thermal generation and distribution within the material using microwave radiation. This can be achieved by developing a coupled electromagnetic and heat transfer model, which will enable a better understanding of the heating mechanisms involved. Furthermore, exploring the micromechanical properties of asphalt concrete during the damage-healing-damage cycle can provide valuable insights. Studying the changes in mechanical properties and damage evolution during the healing process can aid in the development of more advanced and efficient healing mechanisms for asphalt pavement. These future research directions can contribute to further advancements in microwave-heating healing techniques in asphalt composite and pave the way for the development of more sustainable and resilient asphalt pavements.

Acknowledgement

The authors sincerely acknowledge the funding support from Hong Kong Research Grant Council through the GRF project 15209920.

Reference

Test methods of aggregates for highway engineering (JTG E42-2005), China Communications Publishing Press, Beijing, China, 2005.

Amani, S., Jahangiri, B., Karimi, M.M., 2023. Performance characterization of asphalt mixtures under different aging levels: A fracture-based method. Construction and Building Materials 383.http://dx.doi.org/10.1016/j.conbuildmat.2023.131126

Amani, S., Kavussi, A., Karimi, M.M., 2020. Effects of aging level on induced heating-healing properties of asphalt mixes. Construction and Building Materials 263.http://dx.doi.org/10.1016/j.conbuildmat.2020.120105

Anupam, B.R., Sahoo, U.C., Chandrappa, A.K., 2022. A methodological review on self-healing asphalt pavements. Construction and Building Materials 321.http://dx.doi.org/10.1016/j.conbuildmat.2022.126395

Apeagyei, A.K., Grenfell, J.R.A., Airey, G.D., 2014. Observation of reversible moisture damage in asphalt mixtures. Construction and Building Materials 60, 73-80.http://dx.doi.org/10.1016/j.conbuildmat.2014.02.033

Ashish, P.K., Sreeram, A., Xu, X., Chandrasekar, P., Jagadeesh, A., Adwani, D., Padhan, R.K., 2023. Closing the Loop: Harnessing waste plastics for sustainable asphalt mixtures – A comprehensive review. Construction and Building Materials 400.http://dx.doi.org/10.1016/j.conbuildmat.2023.132858

Eisa, M.S., Mohamady, A., Basiouny, M.E., Abdulhamid, A., Kim, J.R., 2022. Mechanical properties of asphalt concrete modified with carbon nanotubes (CNTs). Case Studies in Construction Materials 16.http://dx.doi.org/10.1016/j.cscm.2022.e00930

Franesqui, M.A., Yepes, J., García-González, C., 2017. Top-down cracking self-healing of asphalt pavements with steel filler from industrial waste applying microwaves. Construction and Building Materials 149, 612-620.http://dx.doi.org/10.1016/j.conbuildmat.2017.05.161

García, Á., 2012. Self-healing of open cracks in asphalt mastic. Fuel 93, 264-272.http://dx.doi.org/10.1016/j.fuel.2011.09.009

Gong, M., Sun, Y., Chen, J., 2024. Analysis of coupled thermo-mechanical response and damage behaviour of curved ramp bridge deck pavement using a 3D multiscale method. Road Materials and Pavement Design, 1-23.http://dx.doi.org/10.1080/14680629.2024.2310812

Huang, W., Yu, H., Lin, Y., Zheng, Y., Ding, Q., Tong, B., Wang, T., 2022. Energy analysis for evaluating durability of porous asphalt mixture. Construction and Building Materials 326.http://dx.doi.org/10.1016/j.conbuildmat.2022.126819

Jahanbakhsh, H., Karimi, M.M., Jahangiri, B., Nejad, F.M., 2018. Induction heating and healing of carbon black modified asphalt concrete under microwave radiation. Construction and Building Materials 174, 656-666.http://dx.doi.org/10.1016/j.conbuildmat.2018.04.002

Jiang, J., Leng, Z., Yang, B., Lu, G., Tan, Z., Han, M., Dong, Z., 2022. Penetration mechanism of the emulsion-based rejuvenator in damaged porous asphalt mixture: Microstructure characterization and 3D reconstruction. Materials & Design 221.http://dx.doi.org/10.1016/j.matdes.2022.111014

Jiang, X., Gabrielson, J., Huang, B., Bai, Y., Polaczyk, P., Zhang, M., Hu, W., Xiao, R., 2022. Evaluation of inverted pavement by structural condition indicators from falling weight deflectometer. Construction and

Building Materials 319.http://dx.doi.org/10.1016/j.conbuildmat.2021.125991

Jiang, X., Zhang, M., Xiao, R., Polaczyk, P., Bai, Y., Huang, B., 2021. An investigation of structural responses of inverted pavements by numerical approaches considering nonlinear stress-dependent properties of unbound aggregate layer. Construction and Building Materials 303.http://dx.doi.org/10.1016/j.conbuildmat.2021.124505

Karimi, M.M., Amani, S., Jahanbakhsh, H., Jahangiri, B., Alavi, A.H., 2021. Induced heating-healing of conductive asphalt concrete as a sustainable repairing technique: A review. Cleaner Engineering and Technology 4.http://dx.doi.org/10.1016/j.clet.2021.100188

Karimi, M.M., Jahanbakhsh, H., Jahangiri, B., Moghadas Nejad, F., 2018. Induced heating-healing characterization of activated carbon modified asphalt concrete under microwave radiation. Construction and Building Materials 178, 254-271.http://dx.doi.org/10.1016/j.conbuildmat.2018.05.012

Leclerc, N., Meux, E., Lecuire, J.-M., 2003. Hydrometallurgical extraction of zinc from zinc ferrites. Hydrometallurgy 70(1-3), 175-183.http://dx.doi.org/10.1016/s0304-386x(03)00079-3

Li, C., Wu, S., Chen, Z., Tao, G., Xiao, Y., 2018a. Enhanced heat release and self-healing properties of steel slag filler based asphalt materials under microwave irradiation. Construction and Building Materials 193, 32-41.http://dx.doi.org/10.1016/j.conbuildmat.2018.10.193

Li, C., Wu, S., Chen, Z., Tao, G., Xiao, Y., 2018b. Improved microwave heating and healing properties of bitumen by using nanometer microwave-absorbers. Construction and Building Materials 189, 757-767.http://dx.doi.org/10.1016/j.conbuildmat.2018.09.050

Liu, D., Zhang, H., Liu, Z., Liu, D., He, D., Yu, T., 2023. The heat flux evolution of porous asphalt mixture based on meso-structure and its influence on heat transfer property. Thermal Science and Engineering Progress 43.http://dx.doi.org/10.1016/j.tsep.2023.102020

Liu, J., Chen, S., Liu, Q., Wang, Y., Yu, B., 2022. Influence of steel slag incorporation on internal skeletal contact characteristics within asphalt mixture. Construction and Building Materials 352.http://dx.doi.org/10.1016/j.conbuildmat.2022.129073

Liu, J., Wang, Z., Jia, H., Jing, H., Chen, H., Zhou, L., Yuan, L., Hoff, I., 2023. Characteristics and properties of asphalt mortar containing FO filler. Construction and Building Materials 392.http://dx.doi.org/10.1016/j.conbuildmat.2023.132039

Liu, J., Wang, Z., Li, M., Wang, X., Wang, Z., Zhang, T., 2022. Microwave heating uniformity, road performance and internal void characteristics of steel slag asphalt mixtures. Construction and Building Materials 353.http://dx.doi.org/10.1016/j.conbuildmat.2022.129155

Liu, Q., Wu, S., Schlangen, E., 2013. Induction heating of asphalt mastic for crack control. Construction and Building Materials 41, 345-351.http://dx.doi.org/10.1016/j.conbuildmat.2012.11.075

Liu, Q., Yu, W., Wu, S., Schlangen, E., Pan, P., 2017. A comparative study of the induction healing behaviors of hot and warm mix asphalt. Construction and Building Materials 144, 663-670.http://dx.doi.org/10.1016/j.conbuildmat.2017.03.195

Lou, B., Sha, A., Barbieri, D.M., Liu, Z., Zhang, F., 2021. Microwave heating properties of steel slag asphalt mixture using a coupled electromagnetic and heat transfer model. Construction and Building Materials 291.http://dx.doi.org/10.1016/j.conbuildmat.2021.123248

Lou, B., Sha, A., Li, Y., Wang, W., Liu, Z., Jiang, W., Cui, X., 2020. Effect of metallic-waste aggregates on

484 microwave self-healing performances of asphalt mixtures. Construction and Building Materials
485 246.http://dx.doi.org/10.1016/j.conbuildmat.2020.118510

486 Lu, D., Huo, Y., Jiang, Z., Zhong, J., 2023a. Carbon nanotube polymer nanocomposites coated aggregate
487 enabled highly conductive concrete for structural health monitoring. Carbon 206, 340-
488 350.http://dx.doi.org/10.1016/j.carbon.2023.02.043

489 Lu, D., Jiang, X., Leng, Z., 2024a. Sustainable microwave-heating healing asphalt concrete fabricated with
490 waste microwave-sensitive fillers. Journal of Cleaner Production
491 434.http://dx.doi.org/10.1016/j.jclepro.2023.140343

492 Lu, D., Jiang, X., Leng, Z., Zhang, S., Wang, D., Zhong, J., 2023b. Dual responsive microwave heating-
493 healing system in asphalt concrete incorporating coal gangue and functional aggregate. Journal of Cleaner
494 Production 422.http://dx.doi.org/10.1016/j.jclepro.2023.138648

495 Lu, D., Jiang, X., Qu, F., Huo, Y., 2024b. Mitigating sulfate ions migration in concrete: A targeted approach
496 to address recycled concrete Aggregate's impact. Journal of Cleaner
497 Production.http://dx.doi.org/10.1016/j.jclepro.2024.141135

498 Lu, D., Jiang, X., Tan, Z., Yin, B., Leng, Z., Zhong, J., 2023c. Enhancing sustainability in pavement
499 Engineering: A-state-of-the-art review of cement asphalt emulsion mixtures. Cleaner Materials
500 9.http://dx.doi.org/10.1016/j.clema.2023.100204

501 Lu, D., Leng, Z., Lu, G., Wang, D., Huo, Y., 2023d. A critical review of carbon materials engineered
502 electrically conductive cement concrete and its potential applications. International Journal of Smart and
503 Nano Materials, 1-27.http://dx.doi.org/10.1080/19475411.2023.2199703

504 Lu, D., Shi, X., Zhong, J., 2022. Interfacial bonding between graphene oxide coated carbon nanotube fiber
505 and cement paste matrix. Cement and Concrete Composites
506 134.http://dx.doi.org/10.1016/j.cemconcomp.2022.104802

507 Ma, T., Wang, H., Zhang, D., Zhang, Y., 2017. Heterogeneity effect of mechanical property on creep
508 behavior of asphalt mixture based on micromechanical modeling and virtual creep test. Mechanics of
509 Materials 104, 49-59.http://dx.doi.org/10.1016/j.mechmat.2016.10.003

510 Ma, X., Jiang, J., Zhao, Y., Wang, H., 2021. Characterization of the interconnected pore and its relationship
511 to the directional permeability of porous asphalt mixture. Construction and Building Materials
512 269.http://dx.doi.org/10.1016/j.conbuildmat.2020.121233

513 Mojabi, S.A., Abdi kordani, A., Mirbaha, B., 2020. Laboratory investigation of stone matrix asphalt
514 modified with SBS polymer and C25 fiber in using the semi-circular bend geometry (SCB) and moisture
515 susceptibility. Construction and Building Materials
516 261.http://dx.doi.org/10.1016/j.conbuildmat.2020.120511

517 Nabiun, N., Khabiri, M.M., 2016. Mechanical and moisture susceptibility properties of HMA containing
518 ferrite for their use in magnetic asphalt. Construction and Building Materials 113, 691-
519 697.http://dx.doi.org/10.1016/j.conbuildmat.2016.03.058

520 Phan, T.M., Park, D.-W., Le, T.H.M., 2018. Crack healing performance of hot mix asphalt containing steel
521 slag by microwaves heating. Construction and Building Materials 180, 503-
522 511.http://dx.doi.org/10.1016/j.conbuildmat.2018.05.278

523 Schlangen, E., Sangadji, S., 2013. Addressing Infrastructure Durability and Sustainability by Self Healing

Mechanisms - Recent Advances in Self Healing Concrete and Asphalt. Procedia Engineering 54, 39-57.http://dx.doi.org/10.1016/j.proeng.2013.03.005

Tan, Y., Shan, L., Richard Kim, Y., Underwood, B.S., 2012. Healing characteristics of asphalt binder. Construction and Building Materials 27(1), 570-577.http://dx.doi.org/10.1016/j.conbuildmat.2011.07.006

Wan, P., Wu, S., Liu, Q., Wang, H., Gong, X., Zhao, Z., Xu, S., Jiang, J., Fan, L., Tu, L., 2023. Extrinsic self-healing asphalt materials: A mini review. Journal of Cleaner Production 425.http://dx.doi.org/10.1016/j.jclepro.2023.138910

Wang, Y.-Y., Tan, Y.-Q., Lv, H.-J., Han, M.-Z., 2022. Evaluation of rheological and self-healing properties of asphalt containing microcapsules modified with graphene. Construction and Building Materials 357.http://dx.doi.org/10.1016/j.conbuildmat.2022.129287

Xu, G., Wang, H., 2016. Study of cohesion and adhesion properties of asphalt concrete with molecular dynamics simulation. Computational Materials Science 112, 161-169.http://dx.doi.org/10.1016/j.commatsci.2015.10.024

Xu, S., García, A., Su, J., Liu, Q., Tabaković, A., Schlangen, E., 2018. Self-Healing Asphalt Review: From Idea to Practice. Advanced Materials Interfaces 5(17).http://dx.doi.org/10.1002/admi.201800536

Yang, C., Wu, S., Xie, J., Amirkhanian, S., Liu, Q., Zhang, J., Xiao, Y., Zhao, Z., Xu, H., Li, N., Wang, F., Zhang, L., 2022. Enhanced induction heating and self-healing performance of recycled asphalt mixtures by incorporating steel slag. Journal of Cleaner Production 366.http://dx.doi.org/10.1016/j.jclepro.2022.132999

Yang, H., Ouyang, J., Jiang, Z., Ou, J., 2023. Effect of fiber reinforcement on self-healing ability of asphalt mixture induced by microwave heating. Construction and Building Materials 362.http://dx.doi.org/10.1016/j.conbuildmat.2022.129701

Yoo, D.-Y., Kim, S., Kim, M.-J., Kim, D., Shin, H.-O., 2019. Self-healing capability of asphalt concrete with carbon-based materials. Journal of Materials Research and Technology 8(1), 827-839.http://dx.doi.org/10.1016/j.jmrt.2018.07.001

Zhu, H., Yuan, H., Liu, Y., Fan, S., Ding, Y., 2020. Evaluation of Self-Healing Performance of Asphalt Concrete for Macrocracks via Microwave Heating. Journal of Materials in Civil Engineering 32(9).http://dx.doi.org/10.1061/(asce)mt.1943-5533.0003332

Zhu, X., Cai, Y., Zhong, S., Zhu, J., Zhao, H., 2017. Self-healing efficiency of ferrite-filled asphalt mixture after microwave irradiation. Construction and Building Materials 141, 12-22.http://dx.doi.org/10.1016/j.conbuildmat.2017.02.145

Zhu, X., Fan, Y., Yu, Y., Gilabert, F.A., 2020. Crack propagation and microwave healing of Ferrite-filled asphalt mixes based on image correlation observations. Construction and Building Materials 262.http://dx.doi.org/10.1016/j.conbuildmat.2020.119978

Zhu, X., Ye, F., Cai, Y., Birgisson, B., Lee, K., 2019. Self-healing properties of ferrite-filled open-graded friction course (OGFC) asphalt mixture after moisture damage. Journal of Cleaner Production 232, 518-530.http://dx.doi.org/10.1016/j.jclepro.2019.05.353